Lab on a Chip

Accepted Manuscript

This is an *Accepted Manuscript*, which has been through the Royal Society of Chemistry peer review process and has been accepted for publication.

Accepted Manuscripts are published online shortly after acceptance, before technical editing, formatting and proof reading. Using this free service, authors can make their results available to the community, in citable form, before we publish the edited article. We will replace this *Accepted Manuscript* with the edited and formatted *Advance Article* as soon as it is available.

You can find more information about *Accepted Manuscripts* in the Information for Authors.

Please note that technical editing may introduce minor changes to the text and/or graphics, which may alter content. The journal's standard Terms & Conditions and the Ethical guidelines still apply. In no event shall the Royal Society of Chemistry be held responsible for any errors or omissions in this *Accepted Manuscript* or any consequences arising from the use of any information it contains.

ROYAL SOCIETY OF CHEMISTRY

www.rsc.org/loc

Lab on a Chip

RSCPublishing

ARTICLE

Dynamic formation of a microchannel array enables kinesin-driven microtubule transport between separate compartments on a chip

Cite this: DOI: 10.1039/x0xx00000x

Received 00th January 2012,
Accepted 00th January 2012

DOI: 10.1039/x0xx00000x

www.rsc.org/

Kazuya Fujimoto[a], Moeto Nagai[b], Hirofumi Shintaku[a], Hidetoshi Kotera[a] and Ryuji Yokokawa[a]

Microtubules driven by kinesin motors have been utilised as "molecular shuttles" in microfluidic environments with potential applications in autonomous nanoscale manipulations such as capturing, separating, and/or concentrating biomolecules. However, the conventional flow cell–based assay has difficulty in separating bound from free target molecules even with buffer flushing because the molecular manipulations by molecular shuttles take place on a glass surface and molecular binding occurs stochastically; this makes it difficult to determine whether molecules are carried by molecular shuttles or by diffusion. To address this issue, we developed a microtubule-based transport system between two compartments connected by a single-micrometre-scale channel array that forms dynamically via pneumatic actuation of a polydimethylsiloxane membrane. The device comprises three layers—a control channel layer (top), a microfluidic channel layer (middle), and a channel array layer (bottom)—that enable selective injection of assay solutions to a target compartment and dynamic formation of the microchannel array. The pneumatic channel also serves as a nitrogen supply path to the assay area, which reduces photobleaching of fluorescent labelled microtubules and deactivation of kinesin by oxygen radicals. The channel array suppresses cross-contamination of molecules caused by diffusion or pressure-driven flow between compartments, facilitating unidirectional transport of molecular shuttles from one compartment to another. The method demonstrates, for the first time, efficient and unidirectional microtubule transport by eliminating diffusion of target molecules on a chip and thus may constitute one of the key aspects of motor-driven nanosystems.

Lab on a Chip Accepted Manuscript

Introduction

Since the proposal of micro total analysis systems (μTAS) or lab-on-a-chip,[1] control of fluidic samples in micrometer-scale environments has advanced rapidly owing to the utilisation of micro fabrication techniques.[2] Various functional microfluidic devices have been developed for chemical analysis, medical diagnosis, and other purposes, demonstrating their advantages such as small sample volume and short assay time.[3] Although pressure-driven flow is prevalent for molecular manipulations in μTAS applications, direct manipulation of target molecules is also important for further downsizing of devices because handling extremely small volumes of solution is challenging when using pressure-driven flow. Therefore, electrokinetic manipulation of molecules by external fields has been extensively studied for the purpose of concentrating or separating molecules.[4-6]

In the last decade, many researchers have established novel molecular transport schemes via use of motor proteins. Motor proteins directly convert chemical energy into mechanical work on the molecular scale, implying that nanosysms can be supported by autonomous motor-driven manipulations.[7] The motor protein system comprising kinesin (motor) and microtubules (MTs) plays important roles in intracellular vesicular transport and in regulating cell division in eukaryotes.[8,9] Amongst the various artificial motor protein systems used currently, the combination of kinesin/MTs is widely used in a geometry called "gliding assay" in which MTs glide on a kinesin-coated surface.[10,11] Regarding MTs as "molecular shuttles", molecules can be directly carried on MTs and transported by kinesin motility via ATP hydrolysis in vitro. The integration of micro/nano fabrication and molecular bionanotechnology makes it possible to load/unload and control the directionality of molecular transport. Various binding mechanisms have been employed for cargo loading onto MTs, such as the biotin-streptavidin interaction,[12] DNA hybridisation[13-16], and antigen-antibody recognition.[17–19] Both the direction and location of molecular gliding have been controlled by microfabricated structures,[20–24] and/or by applying

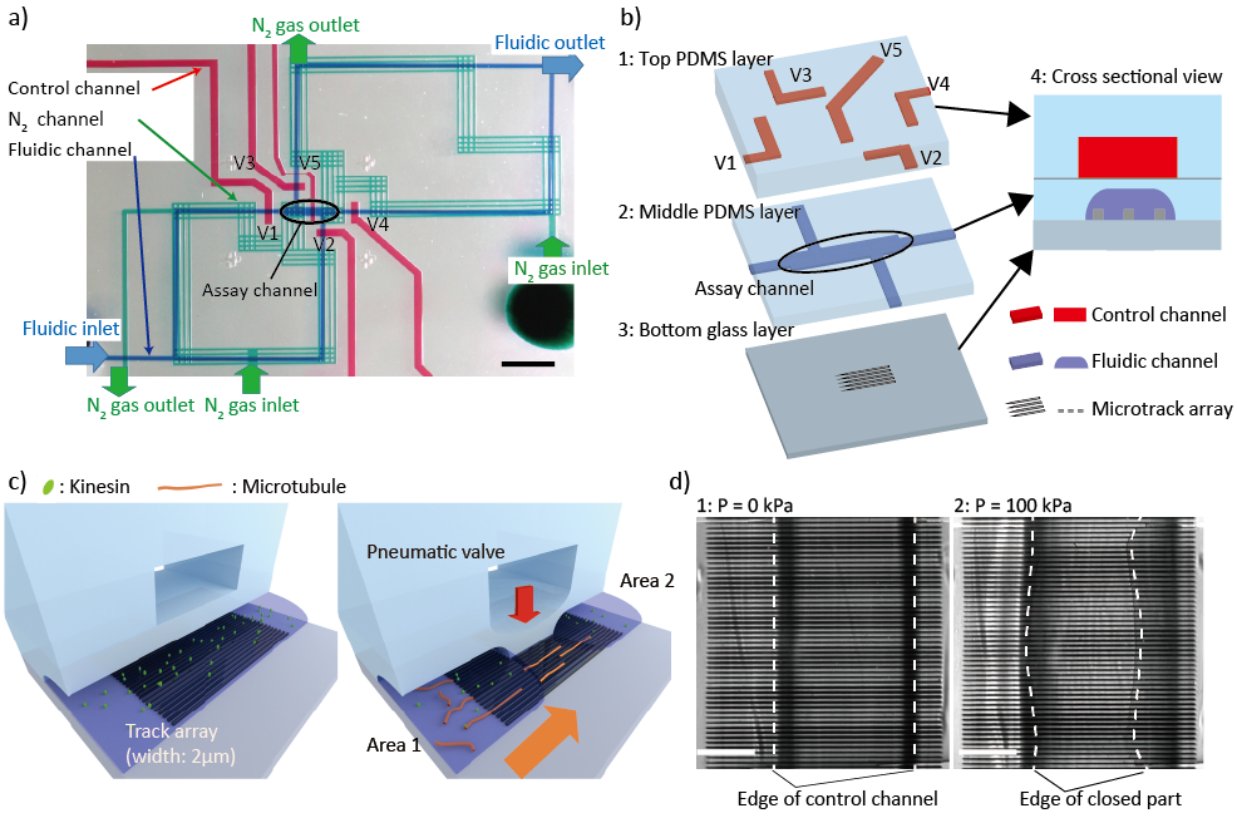

Fig. 1 Fabricated device and its functions. a) Overview of the device. Control channel, fluidic channel, and N_2 channel are coloured red, blue, and green, respectively. The microtrack array patterned on the glass cover slip is located at the centre (enclosed by a circle). Scale bar, 2 mm. b) Three-layer microfluidic device. b-1) Control channel (red) are fabricated on the top PDMS layer. b-2) Fluidic channel (blue) are moulded on the second PDMS layer, of which the channel top is composed of a thin PDMS membrane for pneumatic actuation. b-3) Microtrack array (gray) is patterned on a glass cover slip. b-4) These three layers are bonded together as illustrated. c) Schematic of dynamic formation of a microchannel array. After kinesin molecules are immobilised on the glass surface, the top PDMS membrane is pneumatically actuated, resulting in the formation of the closed channel array. d-1) The microtrack array aligned to a control channel. Without applied pressure, edges of the control channel are clearly observed (white dotted lines). d-2) With applied pressure of 100 kPa, the PDMS membrane compresses and forms the channel array. White dotted lines indicate the boundary of the closed area. Scale bar, 50 μm.

external forces such as an electric field,[25–28] magnetic field,[29] or shear flow.[30–32] Recently, polymer patterning on a substrate for selective immobilisation of kinesin has also been reported.[33–35] Moreover, the integration of cargo loading and subsequent control of transport direction have demonstrated the utility of achieving molecular separations or concentration by molecular shuttles.[36,37]

The next challenge in molecular shuttle applications is to realise autonomous sample processing relying on fewer external manipulations such as sequential exchange of solutions. Bachand *et al.* proposed a device concept consisting of multiple separate modules, in which MTs autonomously and sequentially carry target molecules from the loading module to the tagging and detection modules.[38] In this concept, target molecules must be transported across separate modules filled with different solutions without cross-contamination. However, such molecular transport is not trivial because injecting solutions into individual modules is extremely challenging and diffusion of molecules causes cross-contamination. Kim *et al.* tackled this issue using laminar flow sandwiched by two sheath flows, where streptavidin molecules were captured on biotin-labelled MTs and concentrated.[39] More recently, Steuerwald *et al.* also utilised laminar flows to sequentially load streptavidin and DNA molecules onto MTs via their gliding in two adjacent flows—flow containing streptavidin and the other DNA.[40] MT gliding across separate regions has been thus reported utilising continuous laminar flows, but several shortcomings hamper building a more functional device. Most importantly, it remains challenging to identify the driving force of nanotransport of target molecules because it is not easy to segregate the active transport of molecular shuttles from diffusion-mediated transport and pressure-driven flow in a flow cell–based assay. In addition, laminar flow needs to be maintained throughout the assay via laborious external control by syringe pumps. A high flow rate causes MT detachment from the device surface, thereby decreasing the efficiency of transport.[40]

Here we propose the microfluidic system that enables MT-based transport between two compartments which are physically

Lab on a Chip Accepted Manuscript

 This journal is © The Royal Society of Chemistry 2012

separated. We used a three-layer microfluidic device to assay MTs under a fluidically static condition without pressure-driven flow (Fig. 1a, b). The device enables MTs to glide between physically separate compartments (area 1 and area 2) through a single-micrometre-scale channel array while eliminating the diffusion of cargo molecules or MTs in bulk solution. Selective injection of buffer solutions by pneumatic valves and high fluidic resistance keep distinct sets of molecules in two separate compartments. Pneumatic channels were also utilised to supply nitrogen gas to extend lifetimes of MTs and kinesin.

Material and methods

Design of microfluidic device

The device is constructed of two poly (dimethylsiloxane) (PDMS) layers and a bottom glass cover slip (Fig. 1b). Control channels in the top PDMS layer (Fig. 1b-1) actuate thin PDMS membranes in the middle layer (Fig. 1b-2) to control the direction of buffer solution flow, as reported.[41,42] In addition to such conventional use of pneumatic control channels, they have two unique functions in our device. First, one of the control channels serves to dynamically create the channel array during an assay by compressing the PDMS membrane on the microtrack array fabricated on the cover slip (Fig. 1b-3, 4, and Fig. 1c). Quick and easy formation of the channel array facilitates easy buffer perfusions with less hydraulic resistance before forming the channel array. This method promotes MT gliding in the single-micrometre-scale channel array of 2 μm in width and ~0.7 μm in height, a channel size that has made assays laborious owing to a large pressure drop.[43–46] Second, nitrogen gas (N_2) is supplied to the assay channel area, which extends the assay time by reducing photobleaching and protein deactivation via reaction with oxygen radicals.[47]

Microfluidic device fabrication

Top PDMS layer with control channels: A mould for control channels was fabricated by UV photolithography of an SU-8 3050 resist (MicroChem) on a silicon substrate (see ESI† for details of mould fabrication). PDMS prepolymer mixed with a curing agent (SILPOT 184 W/C, Dow Corning Toray) at 10:1 w/w was cast on the mould with thickness ~10 mm. It was degassed in a vacuum chamber for 1 hr, cured at 80°C for 1 hr, and removed from the mould. Inlet and outlet holes used for the external pressure source and N_2 supply were punched by a biopsy (Sterile Dermal Biopsy Punch, 3 mm, Kai Industry).

Middle PDMS layer with fluidic channels sealed by a thin PDMS membrane: An AZP4903 (AZ electronic) photoresist patterned on silicon substrate was employed as the mould for fluidic channels. Following the photolithography process, the photoresist was reflowed at 150°C for 2 hr to produce round cross-sections. The dimensions of the resulting resist shapes were measured by a surface profiler before and after reflow (Fig. S1), and a finite element model simulation with MemsONE software (Micromachine Centre, Japan) was conducted to examine if the rounded cross-sections were suitable for valve closure[48] (Fig. S2). PDMS prepolymer and curing agent were mixed at a ratio of 20:1, and 0.2 g of a wetting agent (501W additive, Dow Corning) per 10 g mixture was added. The mixture was spin-coated on the mould at 2000 rpm for 60 s (K359S1, Kyowariken) to obtain a 60-μm-thick PDMS membrane that was then cured at 80°C for 1 hr.

Bottom cover slip with microtrack array: An aluminium layer was deposited on a borosilicate cover slip (24 × 36 mm, No. 1 thickness, Matusnami) after cleaning in a piranha solution (mixture of sulphuric acid and hydrogen peroxide, 3:1 v/v). The aluminum thickness was monitored during the thermal deposition to obtain ~150 nm. An SU-8 2000.5 resist (MicroChem) was then spin-coated (1H-D7, Mikasa) and patterned using a double-sided mask aligner (PEM800, Union). An array of microtracks (2 μm of width in design) was fabricated by developing the SU-8 layer in SU-8 developer (MicroChem) and etching the aluminum layer. Width of etched microtracks was measured as 2.1 ± 0.1 μm (mean ± SD) from microscope images. The total height of the aluminum layer and the SU-8 layer was 0.7 ± 0.07 μm, which was measured by a surface profilometer (Dektak XT-S, Veeco). The etching was implemented immediately before device assembly to utilise the clean glass surface for uniform immobilisation of kinesin. This is because we found that some MTs did not glide smoothly when the cover slip was stored for >2 days after the aluminium etching process.

Device assembly: The top PDMS layer was first bonded with the middle PDMS layer after an air plasma exposure (COVANCE MP, FEMTO Science). The middle PDMS layer remained attached to the silicon wafer; the bonding was completed by curing for 1 hr at 80°C. The two bonded PDMS layers were then peeled from the fluidic channel mould. Holes of 3 mm in diameter were punched in the PDMS slab to serve as the solution inlet and outlet, and the slab was bonded to the bottom glass cover slip activated by an air plasma exposure. Finally, the device was cured for 1 hr at 80°C to reduce the prepolymers remained not cured and reinforce the bonding strength. Control channels were connected to an external pressure source, and the supply of pressure was individually controlled through each channel by an electromagnetic valve and digital regulator (ARP20K-02, SMC). Before applying pressure, the PDMS membrane on top of the microchannel array was not deformed (Fig. 1d-1). Once 100 kPa of pressure was applied to the control channel, the membrane in the middle PDMS layer was deformed to seal the top of the microtracks fabricated on the bottom cover slip (Fig. 1d-2).

Protein preparation

The kinesin construct consisted of sequence encoding human kinesin amino acid residues 1–573 with a 6-residue N-terminal histidine tag, which was purified by chelating to nickel-coupled resin as described.[49] Tubulin was purified from porcine brain as described,[50] which yielded 5–6 mg mL^{-1} tubulin solution. Purified tubulin was fluorescently labelled by conjugating with tetramethyl rhodamine (C1171, Molecular Probes). Kinesin,

Lab on a Chip Accepted Manuscript

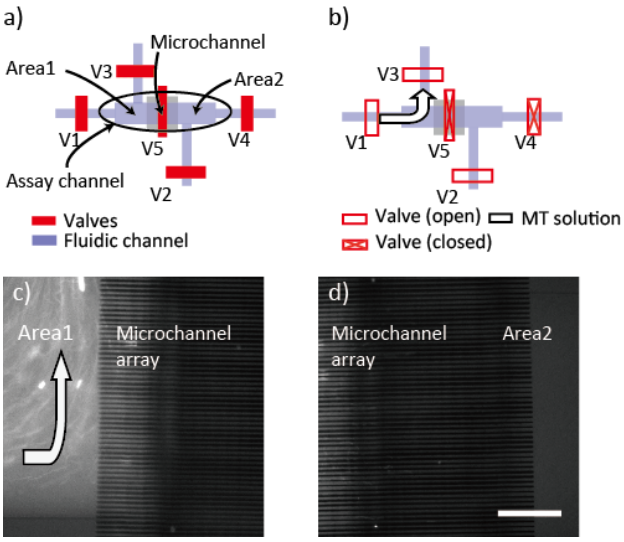

Fig. 2 Selective injection of buffer solutions by actuating pneumatic valves. a) Schematic of the flow control. Liquid flow to the assay channel is controlled by four valves (valves 1–4). Valve 5 forms the microchannel array. b) Upon introduction of MT solution, valves 4 and 5 are closed to selectively introduce MTs into area 1. c) MT introduction. MTs were selectively introduced into area 1, but not into the microchannel array. Flow direction is visualised by aligned MTs in the flow direction indicated by the white arrow. d) MTs were not observed in the microchannel area and area 2 because MT diffusion was suppressed by valve operation. Scale bar, 50 µm.

tubulin, and fluorescently labelled tubulin were aliquoted into sample tubes and stored in liquid nitrogen. Labelled MTs were polymerised by mixing non-labelled tubulin and labelled tubulin at a molar ratio of 10:1 and polymerised at 37°C for 45 min in the presence of 0.5 mM $MgSO_4$ and 0.5 mM GTP. Solution containing polymerised MT solution was stored at room temperature after adding 4 µM Taxol as a stabilising agent and used within one week.

Motility assay

Before starting the assay, the device was degassed in a vacuum chamber for 1 hr. Assay solutions were sequentially introduced to the assay channel with valve operations to achieve selective immobilisation of proteins in the target area (Fig. 2a). Immediately after the device was removed from the chamber, fluid inlet and outlet holes were filled with 2 mg mL^{-1} Pluronic F108 (BASF) solution with all valves 1–5 open (Fig. S3a). The solution was autonomously introduced into fluidic channels by negative pressure, and then Pluronic F108 was rinsed out with BRB80 buffer (80 mM PIPES, 1 mM EGTA, 1 mM $MgSO_4$, pH 6.8) for >3 min. Flow was regulated by the head difference (~5 mm) between the fluid inlet and outlet. Kinesin solution, diluted to 70 µg mL^{-1} in BRB80 containing 0.2 mg mL^{-1} casein, was then introduced via the fluid inlet (Fig. S3b). To ensure kinesin immobilisation, the flow was maintained for 10 min followed by a 3-min incubation by closing valves 1 and 4 (Fig. S3c). The kinesin solution was washed out by flowing BRB80 for 3 min with valves 1, 4, and 5 open (Fig. S3d). Valves 4 and 5 were closed before MT solution was introduced to immobilise MTs only in area 1 (Fig. 2b, c and Fig. S3e). The MT solution was prepared at a tubulin dimer concentration of 120 µg mL^{-1} in BRB80 containing 1 mM ATP, 4 µM Taxol, and an oxygen scavenging system (36 µg mL^{-1} catalase, 25 mM glucose, 216 µg mL^{-1} glucose oxidase, 1% β-mercaptoethanol, 0.2 mg mL^{-1} casein, and 20 mM dithiothreitol). At this stage, we confirmed that no MTs were introduced to the channel array or area 2 by pressure-driven flow (Fig. 2d) and observed that MTs started gliding. During the assay, fluid flow was continuously supplied to area 1 by opening valves 1 and 2, while flow in area 2 was stopped by closing valve 4 (Fig. S3e). Valve 2 was kept open to avoid

Stable MT motility by supplying N_2

N_2 was supplied via two N_2 inlets and vented via two outlets as indicated by green arrows in Fig. 1a. Gas flow was supplied for 30 min before starting the assay and was maintained during the assay. Gas pressure was maintained at 10 kPa, which was substantially lower than the pressure required to control the valve (~100 kPa) so as to avoid unexpected closure or deformation of fluidic channels.

Imaging and data processing

Gliding of labelled MTs and Brownian motion of quantum dots (Q-dots) (Q10121MP, Invitrogen) were visualised via fluorescence microscopy (IX 71, Olympus), in which 40× and 100× objective lenses were equipped for MT and Q-dot observations, respectively. Images were recorded by an electron multiplying charge-coupled device camera (iXon EM+ DU-897, Andor Technology PLC) connected to a PC. An exposure time of 400 ms and electron-multiplying gain of 299 with a neutral density 6 filter were used throughout the MT assay. MTs velocities were measured using Mark2 software.[51] MTs were counted using ImageJ (National Institute of Health) and lines8 plugin.

When Brownian motion of Q-dots was observed in the microchannel array, the exposure time was reduced to 10 ms for higher temporal resolution. Q-dots were tracked using FIESTA software[52] from sequential TIFF images. Obtained trajectories were further analysed with Matlab 2013b (MathWorks).

Results and discussion

Dynamic formation of the microchannel array

Complete closure of the channel array was verified by observing Brownian motion of Q-dots (1 nM). In the area where the top of the microtrack array was not closed by the PDMS membrane (blue rectangle area in Fig. 3a), Brownian motion of Q-dots was restricted within the track width but not in the out-of-plane direction (*z*-axis direction) (ESI†. Movie 2). This resulted in a short residence time of Q-dots in the viewing area (blue trajectories in Fig. 3a). On the other hand, Q-dots in the microchannel array where the PDMS membrane was compressed showed Brownian motion restricted in both the in-

Lab on a Chip Accepted Manuscript

This journal is © The Royal Society of Chemistry 2012

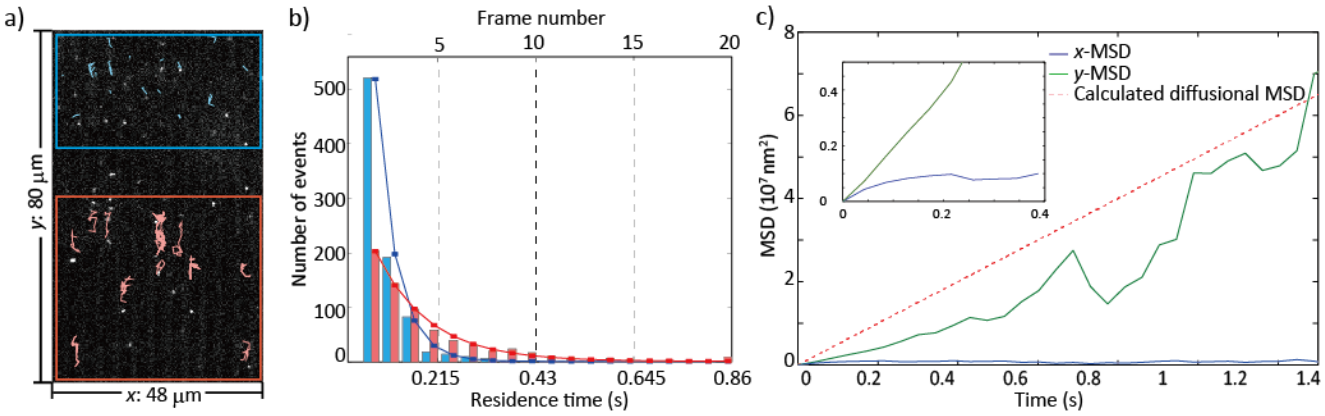

Fig. 3 Evaluation of channel closure. a) Trajectories of Q-dots by Brownian motion. The area enclosed by the blue rectangle corresponds to the microtrack array, *i.e.*, the PDMS membrane is not compressed, where Q-dot trajectories are shown in blue. The microchannel array was formed in the red rectangle area, where Q-dot trajectories are in red. b) Residence time histogram for trajectories obtained in the microtrack array (blue) and the microchannel array (red). The total number of trajectories were 868 and 688 in the microtrack and microchannel arrays, respectively. c) Plots of MSDs. Time course of MSDs along the *x* and *y* directions was calculated from Q-dot trajectories in the microchannel array. Inset is an enlarged view of MSDs from 0 s to 0.4 s. *y*-MSD (green) increased over time and showed a similar trend as the MSD theoretically calculated for free diffusion (red dotted line). However, the *x*-MSD (blue) remained nearly zero.

plane and out-of-plane directions (red rectangle area in Fig. 3a). Therefore, red trajectories in Fig. 3a were longer than those in blue.

Q-dot confinement was quantified. Residence time of Q-dots (*i.e.*, frame number continuously tracked) was measured and plotted in Fig. 3b. Apparently, Q-dots in the microchannel array (red) showed longer residence time than those in the microtrack array (blue). Q-dot tracking was terminated, once Q-dots escaped from the focal depth. Therefore, when Q-dot diffusion was suppressed in the microchannel array, the probability that a Q-dot was observable in two consecutive frames increases. In Fig. 3b, we plotted a histogram of residence time (or frame number; one frame corresponds to 0.043 s) measured from Q-dot trajectories in the microtrack and microchannel arrays. As the residence time is stochastically determined, the histograms are fitted by exponential decay (Fig. 3b) expressed as

$$N_i = N_0 p^{(i-1)}, \qquad (1)$$

where p is the probability that a Q-dot is continuously observed in two frames, i is a frame number, and N_0 is a normalisation factor. Curve fitting to histograms yielded p values of 0.38 and 0.69 for Q-dots in the microtrack and microchannel arrays, respectively. This significant difference in residence time demonstrated that the probability of Q-dot confinement increased in the out-of-plane. In addition, of the 688 Q-dots tracked in the microchannel array, 10 could be observed in more than 20 consecutive frames, corresponding to 1.5% of all the Q-dots. The ratio, 1.5% is $>10^6$ times larger than that calculated for a Q-dot exposed to three-dimensional diffusion. These analyses strongly indicate that Q-dot diffusion in the out-of-plane direction was limited by dynamic formation of the microchannel array.

Q-dot confinement was also evaluated by time development of mean squared displacement (MSD) of each Q-dot trajectory along the *x* and *y* axes defined in Fig. 3a. Two average MSDs in *x* and *y* directions are plotted in Fig. 3c, which were calculated from all the trajectories at each time point. Because the residence time varies as shown in Fig. 3a and 3b, the number of trajectories used for MSD calculation decreased with the elapsed time. For example, MSDs were calculated from 688 trajectories at time = 0 s and from 5 trajectories at time = 1.4 s. In addition, the theoretical MSD calculated for diffusion was also plotted. The *y*-MSD curve showed continuous increase, but the *x*-MSD curve did not increase appreciably over time. The trend of the y-MSD was relatively small compared to that of the theoretical plot (see ESI† for details). This discrepancy can be explained by the hindrance of particle diffusion near the surface. In the condition

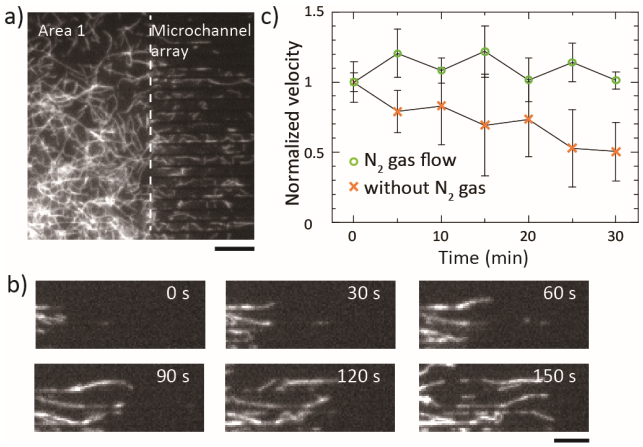

Fig. 4 MT motility in the microchannel array with N_2 flow. a) Overview of gliding MTs in the area 1 side of the microchannel array. Scale bar, 10 µm. b) Sequential images of gliding MTs. Scale bar, 5 µm. c) Time course of gliding velocity with (closed circle) or without N_2 flow (cross). Error bars represents standard deviation of the average from more than five MTs.

Lab on a Chip Accepted Manuscript

where the distance between a particle and a surface is relatively small compared to the particle radius, diffusion coefficient decreases as a function of the ratio. Assuming that the ratio is around 0.2 (10 nm (Q-dot radius) / 50 nm (the distance) for our experimental setup), diffusion coefficient is reported to drop ~80% of that in free diffusion.[53] The inset in Fig. 3c shows an enlargement of the period 0–0.4 s. The observed small MSD along the *x* direction, which is perpendicular to the channel, indicates confinement of Q-dots in the channel. Both residence time and MSD analysis quantitatively prove that the microchannel array was indeed completely sealed upon its formation after actuation of the PDMS membrane.

N_2 flow retains gliding motility in assay channels

In our first trial of the assay in the PDMS device, we noticed that MT velocity drastically decreased after 10–15 min. We attributed this to the high oxygen gas (O_2) permeability of PDMS, because Bruner *et al*. reported deceleration of MTs in <30 s on a PDMS surface under fluorescence excitation owing to damage to both kinesin and MT molecules by reactive oxygen species.[54] Fortunately, an N_2 gas chamber system can preserve MT gliding motility for >10 min in a PDMS flow cell.[55,56], and it was recently reported that photodamage can be minimized in a PDMS micro fluidic device by using an N_2 stream to purge O_2 gas from the PDMS.[57] Therefore, to purge O_2 gas in the PDMS surrounding the assay area, we delivered N_2 through control channels as described in Material and Methods. MT gliding was observed in area 1, and some MTs glided into the microchannel array (Fig. 4a, b). The effect of the method was quantified by measuring MT velocity with or without N_2 flow. The time course of velocity v was normalised by initial velocity v_i and plotted in Fig. 4c. Without N_2 flow, normalised velocity decreased from the initial 1.0 ± 0.14 (v/v_i) (mean ± SD) to 0.50 ± 0.2 (v/v_i) after 30 min. In contrast, MT velocity with N_2 flow did not decrease significantly over 30 min, resulting in an essentially constant normalised velocity of 1.0 ± 0.1 (v/v_i). This result demonstrates the general applicability of the proposed method for the MT assay in any PDMS-based device.

Transport of MTs through the microchannel array

In our initial assays, MTs were first introduced to area 1 only by selective valve operation, and MTs were not observed in area 2 (Fig. 2b, c and Fig. S3d). Many MTs were found on the left (area 1) side of the array at t = 180 s and gradually translocated to the right side (area 2; Fig. 5a). This was also captured as a movie clip (ESI†. Movie 1). This MT motility could not be achieved without valve operation because unbound MTs were observed in the conventional flow cell–based assay. Figures 5b and 5c show the fluorescence intensity profile along each of the two lines A–B (180 s) and A'–B' (720 s) in Fig. 5a. No fluorescence intensity peak, i.e., corresponding to a MT, was detected at 180 s, whereas many peaks were observed at 720 s.

To further evaluate time transition of MTs, we measured the time-course change in MT density in the two regions demarcated by red rectangles in the insets of Figs. 6a and 6b. The former region corresponds to the area in which the microchannel array was formed, and the latter is located in area 2 (exit of the channels). In Fig. 6a, MT density was nearly zero at time t = 0 s and increased until the density reached a maximum. The increase can be explained by the fact that MTs moved from area 1 into the microchannel array where MTs were not initially present. Once the microchannel array was filled with MTs and the numbers of

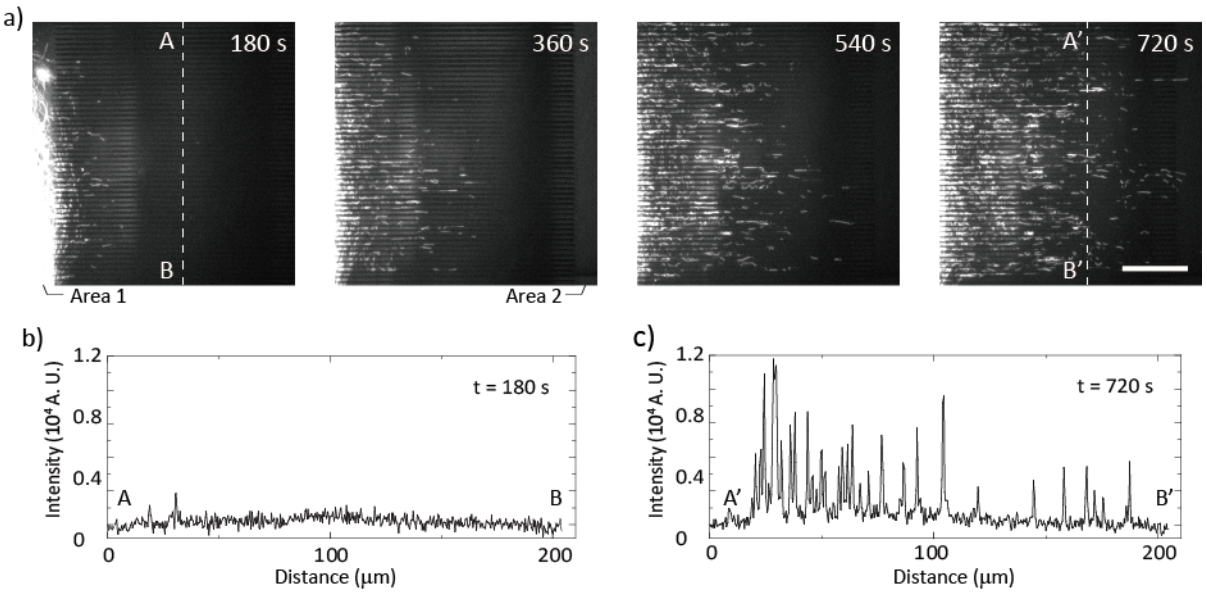

Fig. 5 Transition of MT distribution in the microchannel array over time. a) Sequential images of MTs transiting from area 1 to area 2. After starting the assay, a few MTs glided into microchannels at 180 s. Several MTs reached area 2 at 540 s. More MTs were found in area 2 at 720 s. Scale bar, 50 μm. Fluorescence intensity profile (arbitrary unit, A. U.) along A–B at b) 180 s and A′–B′ at c) 720 s. Many peaks were observed in c) owing to the presence of MTs in the microchannel array.

Lab on a Chip Accepted Manuscript

 This journal is © The Royal Society of Chemistry 2012

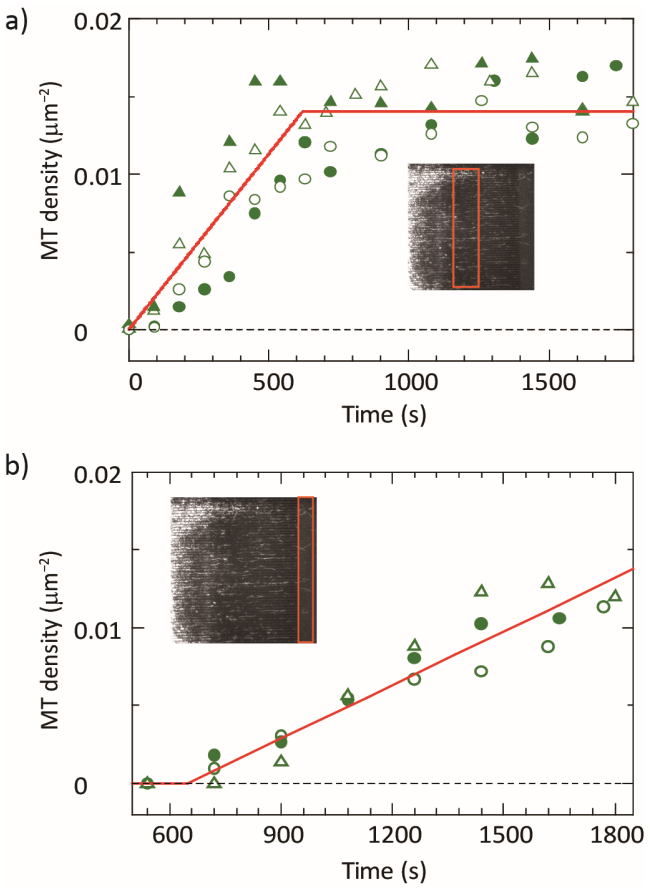

Fig. 6 MT density as a function of time. a) MT density in the microchannel area. MTs were counted within the area enclosed by the orange rectangle. Data in the plots were obtained from four experiments, and curve fitting yielded the red line. b) MT density in area2 was measured by counting the number of MTs within the area enclosed by the orange rectangle. Data were obtained from three experiments and were fitted as noted in panel a.

incoming and outgoing MTs were balanced, MT density was maximal. Based on this idea, the time course of MT density, D_{MT}, was fitted with the equation

$$D_{MT}(t) = \begin{cases} kt\ (t < T) \\ kT (t \geq T) \end{cases}, \quad (2)$$

where k represents the coefficient of the increase in D_{MT}, and T is the time needed to achieve maximal MT density. T was calculated as 6.2×10^2 s by least squares fitting.

Figure 6b shows the time course of MT density in area 2. MTs were not observed in area 2 until t = 700 s**.** The time-course of D_{MT} was fitted by the equation

$$D_{MT}(t) = \begin{cases} 0 & (t < T') \\ k'(t - T')(t \geq T') \end{cases}, \quad (3)$$

where k' is the coefficient of the increase in D_{MT} and T' is the time until the density begins to increase. Values of T' and k' were calculated as 650 s and 1.1×10^{-5} μm^{-2} s^{-1}, respectively. Fitted values, k, T, k' and T', can be used to evaluate the transport effectiveness of the system. For example, the increase rate of MTs in the region of 40.0 × 205 μm (red rectangle, Fig. 6b) was calculated as 9.3×10^{-2} s^{-1}.

This increase of MT density could not be realised without controlling the pressure difference between areas 1 and 2. If this pressure difference was larger than that between valves 1 and 2 (see Fig. 2a, b), selective introduction of MT solution into area 1 was perturbed. For the sake of practicality, the average flow velocity induced by a pressure difference in the channels was calculated by the Darcy-Weisbach equation.[58] For example, assuming that the pressure difference between areas 1 and 2 was 10 Pa, the average velocity in the microchannel array was calculated as 6.2 μm s^{-1}. On the other hand, when the microtrack array was not closed by the PDMS membrane, the average velocity under the same pressure difference was calculated as 3.8 mm s^{-1} (see ESI† for details). This comparison of flow velocity indicates that the microchannel array can serve as a barrier to avoid cross-contamination during solution exchange.

Analysis of active transport and comparison with *in vivo* transport

Compared with the free diffusion of molecules, molecular shuttling—as represented by the active transport of MTs by kinesin—can achieve enhanced and directed transport in microfluidic environments.[11,59] Here, we applied the same idea to our microfluidic device: we calculated the time required to equilibrate the concentrations of MTs in the two areas (compartments) connected with the channel array. Assuming a molecular diameter of 10 nm, area 1 (0.2 nL, 20 μm × 100 μm × 100 μm) was filled with a 1 nM solution of the molecule, and area 2 (same volume as area 1) was free of the molecule; in this scenario, the diffusion-driven transport displaced ~3000 molecules (see ESI† for details) from area 1 to area 2 within 10 min, which is equivalent to 2.5% of all molecules. When active transport is employed, however, the same number of molecules were transported from area 1 to area 2 in the initial ~100 s. Here, we assumed MTs served as cargo transporters[12,60] and carried ~30 cargo molecules s^{-1} on a 10-μm-long MT (see ESI† for details). This comparison clearly indicates that active transport of molecules, rather than their simple diffusion, predominated in the proposed device. The advantage would be further enhanced if target molecules were larger or the solution viscosity was greater, because these parameters result in a smaller diffusion coefficient, yielding a slower rate of transport. This simple calculation demonstrates how active transport potentiates the utility of microfluidic devices.

Conclusion

Here, we realised transitional and unidirectional transport of MTs from MT-supplied area (area 1) to a MT-free area (area 2) that are physically separated in the microfluidic device. The essential functions of the device was to utilise a PDMS membrane to dynamically form the microchannel array from the microtrack array, which was examined by the analysis of Q-dot Brownian motion. Another essential function was to suppress

Lab on a Chip Accepted Manuscript

photobleaching of MTs by delivering N_2 flow through control channels.

Toward sequential molecular analysis utilising MTs as molecular shuttles, the device provides the advantage that target molecules can be handled between adjacent compartments without the help of continuous laminar flow. It allows us to focus on the active transport of MTs. Because the assay was validated in an integrated PDMS microfluidic device, the method has further potential to take advantage of PDMS properties to achieve higher productivity, cost efficiency, and integration with microfluidic components such as a peristaltic pump.[61] The proposed experimental system constitutes a substantial advance toward the development of practical nano/micro-scale fluidic devices driven by motor proteins.

Acknowledgements

This work was supported by a Grant-in-Aid for JSPS Fellows Grant Number 25·1836 to K. F.; KAKENHI Grant Number 25709018 to R. Y.; Kyoto University Supporting Program for Interaction-Based Initiative Team Studies (SPIRITS) to R. Y.

Notes and references

[a]*Department of Micro Engineering, Kyoto University, Kyoto-daigaku Katsura, Nishikyo-ku, Kyoto, 615-8540, Japan.*

[b]*Department of Mechanical Engineering, Toyohashi University of Technology, 1-1 Hibarigaoka, Tenpaku-cho, Toyohashi, Aichi, 441-8580, Japan*

†Electronic Supplementary Information (ESI) available (two videos and one document). See DOI: 10.1039/b000000x/

1 A. Manz, N. Graber and H. M. Widmer, *Sens. Actuators, B*, 1990, **1**, 244-248.
2 H. A. Stone, A. D. Stroock and A. Ajdari, *Annu. Rev. Fluid. Mech.*, 2004, **36**, 381-411.
3 A. Arora, G. Simone, G. B. Salieb-Beugelaar, J. T. Kim and A. Manz, *Anal. Chem.*, 2010, **82**, 4830-4847.
4 J. Fu, R. B. Schoch, A. L. Stevens, S. R. Tannenbaum and J. Han, *Nat Nanotechnol*, 2007, **2**, 121-128.
5 D. W. Inglis, E. M. Goldys and N. P. Calander, *Angew. Chem.*, 2011, **123**, 7688-7692.
6 C. L. Zhao and C. Yang, *Microfluid Nanofluid*, 2012, **13**, 179-203.
7 A. Goel and V. Vogel, *Nat Nanotechnol*, 2008, **3**, 465-475.
8 M. A. Welte, *Curr. Biol.*, 2010, **20**, R410-413.
9 E. Nogales, *Annu. Rev. Biochem.*, 2000, **69**, 277-302.
10 T. Korten, A. Månsson and S. Diez, *Curr. Opin. Biotechnol.*, 2010, **21**, 477-488.
11 H. Hess and V. Vogel, *Rev. Mol. Biotechnol.*, 2001, **82**, 67-85.
12 C. Schmidt, B. Kim, H. Grabner, J. Ries, M. Kulomaa and V. Vogel, *Nano Lett.*, 2012, **12**, 3466-3471.
13 C. Schmidt and V. Vogel, *Lab Chip*, 2010, **10**, 2195-2198.
14 R. Yokokawa, J. Miwa, M. C. Tarhan, H. Fujita and M. Kasahara, *Anal. Bioanal. Chem.*, 2008, **391**, 2735-2743.
15 S. Hiyama, Y. Moritani, R. Gojo, S. Takeuchi and K. Sutoh, *Lab Chip*, 2010, **10**, 2741-2748.
16 M. Lard, L. ten Siethoff, J. Generosi, A. Månsson and H. Linke, *Nano Lett.*, 2014, **14**, 3041-3046.
17 G. D. Bachand, S. B. Rivera, A. Carroll-Portillo, H. Hess and M. Bachand, *Small*, 2006, **2**, 381-385.
18 L. Rios and G. D. Bachand, *Lab Chip*, 2009, **9**, 1005-1010.
19 S. Ramachandran, K.-H. Ernst, G. D. Bachand, V. Vogel and H. Hess, *Small*, 2006, **2**, 330-334.
20 H. Hess, J. Clemmens, D. Qin, J. Howard and V. Vogel, *Nano Lett.*, 2001, **1**, 235-239.
21 H. Hess, C. M. Matzke, R. K. Doot, J. Clemmens, G. D. Bachand, B. C. Bunker and V. Vogel, *Nano Lett.*, 2003, **3**, 1651-1655.
22 Y. Hiratsuka, T. Tada, K. Oiwa, T. Kanayama and T. Q. Uyeda, *Biophys. J.*, 2001, **81**, 1555-1561.
23 S. G. Moorjani, L. Jia, T. N. Jackson and W. O. Hancock, *Nano Lett.*, 2003, **3**, 633-637.
24 J. Clemmens, H. Hess, R. Doot, C. M. Matzke, G. D. Bachand and V. Vogel, *Lab Chip*, 2004, **4**, 83-86.
25 T. Kim, M.-T. Kao, E. F. Hasselbrink and E. Meyhöfer, *Nano Lett.*, 2007, **7**, 211-217.
26 M. Uppalapati, Y.-M. Huang, V. Aravamuthan, T. N. Jackson and W. O. Hancock, *Integr. Biol.*, 2011, **3**, 57-64.
27 M. G. L. van den Heuvel, C. T. Butcher, S. G. Lemay, S. Diez and C. Dekker, *Nano Lett.*, 2005, **5**, 235-241.
28 N. Isozaki, S. Ando, T. Nakahara, H. Shintaku, H. Kotera, E. Meyhöfer and R. Yokokawa, *Scientific reports*, 2015, **5**, 7669-7669.
29 B. M. Hutchins, M. Platt, W. O. Hancock and M. E. Williams, *Small*, 2007, **3**, 126-131.
30 T. Kim, M.-T. Kao, E. Meyhöfer and E. F. Hasselbrink, *Nanotechnology*, 2007, **18**, 025101.
31 R. Yokokawa, S. Takeuchi, T. Kon, M. Nishiura, K. Sutoh and H. Fujita, *Nano Lett.*, 2004, **4**, 2265-2270.
32 R. R. Agayan, R. Tucker, T. Nitta, F. Ruhnow, W. J. Walter, S. Diez and H. Hess, *Langmuir*, 2013, **29**, 2265-2272.
33 L.-J. Cheng, M.-T. Kao, E. Meyhöfer and L. J. Guo, *Small*, 2005, **1**, 409-414.
34 C. Reuther, L. Hajdo, R. Tucker, A. A. Kasprzak and S. Diez, *Nano Lett.*, 2006, **6**, 2177-2183.
35 M. Bhagawati, S. Ghosh, A. Reichel, K. Froehner, T. Surrey and J. Piehler, *Angew. Chem.*, 2009, **48**, 9188-9191.
36 T. Fischer, A. Agarwal and H. Hess, *Nat Nanotechnol*, 2009, **4**, 162-166.
37 C.-T. Lin, M.-T. Kao, K. Kurabayashi and E. Meyhofer, *Nano Lett.*, 2008, **8**, 1041-1046.
38 G. D. Bachand, H. Hess, B. Ratna, P. Satir and V. Vogel, *Lab Chip*, 2009, **9**, 1661-1666.
39 T. Kim, L.-J. Cheng, M.-T. Kao, E. F. Hasselbrink, L. Guo and E. Meyhöfer, *Lab Chip*, 2009, **9**, 1282-1285.
40 D. Steuerwald, S. M. Früh, R. Griss, R. D. Lovchik and V. Vogel, *Lab Chip*, 2014, DOI: 10.1039/c4lc00385c.
41 M. A. Unger, H. P. Chou, T. Thorsen, A. Scherer and S. R. Quake, *Science*, 2000, **288**, 113-116.
42 M. Nagai, S. Ryu, T. Thorsen, P. Matsudaira and H. Fujita, *Lab Chip*, 2010, **10**, 1574-1578.
43 Y.-M. Huang, M. Uppalapati, W. O. Hancock and T. N. Jackson, *Biomed. Microdevices*, 2007, **9**, 175-184.
44 M. G. L. van den Heuvel, M. P. de Graaff and C. Dekker, *Science*, 2006, **312**, 910-914.
45 M. Uppalapati, W. O. Hancock and T. N. Jackson, *IEEE Trans. Adv. Packag.*, 2005, **28**, 564-570.
46 R. Yokokawa, Y. Yoshida, S. Takeuchi, T. Kon and H. Fujita, *Nanotechnology*, 2006, **17**, 289-294.
47 A. M. R. Kabir, D. Inoue, A. Kakugo, K. Sada and J. P. Gong, *Polym. J.*, 2012, **44**, 607-611.
48 Y. Q. Luo and R. N. Zare, *Lab Chip*, 2008, **8**, 1688-1694.
49 R. Yokokawa, M. C. Tarhan, T. Kon and H. Fujita, *Biotechnol. Bioeng.*, 2008, **101**, 1-8.
50 R. C. Williams and J. C. Lee, *Methods Enzymol.*, 1982, **85**, 376-385.
51 K. Furuta, A. Furuta, Y. Toyoshima, Yano, M. Amino, K. Oiwa and H. Kojima, *Proc. Natl. Acad. Sci. U. S. A.*, 2013, **110**, 501-506.
52 F. Ruhnow, D. Zwicker and S. Diez, *Biophys. J.*, 2011, **100**, 2820-2828.
53 B. Lin, J. Yu and S. Rice, *Physical review. E, Statistical physics, plasmas, fluids, and related interdisciplinary topics*, 2000, **62**, 3909-3919.
54 C. Brunner, K. Ernst, H. Hess and V. Vogel, *Nanotechnology*, 2004, **15**, S540-S548.
55 R. M. Lycans, C. B. Higgins, M. S. Tanner, E. R. Blough and B. S. Day, *Colloids Surf., B*, 2014, **116**, 687-694.

Lab on a Chip Accepted Manuscript

 This journal is © The Royal Society of Chemistry 2012

56 A. M. R. Kabir, D. Inoue, A. Kakugo, A. Kamei and J. P. Gong, *Langmuir*, 2011, **27**, 13659-13668.
57 V. Vandelinder and G. D. Bachand, *Anal. Chem.*, 2014, **86**, 721-728.
58 N. Nam-Trung and T. Steven, Wereley, *FUNDAMENTALS AND APPLICATIONS OF MICROFLUIDICS*, ARTECH HOUSE, INC., 685 Canton Street Norwood, MA 02062, 2002.
59 P. Katira and H. Hess, *Nano Lett.*, 2010, **10**, 567-572.
60 G. D. Bachand, S. B. Rivera, A. K. Boal, J. Gaudioso, J. Liu and B. C. Bunker, *Nano Lett.*, 2004, **4**, 817-821.
61 C.-H. Wang and G.-B. Lee, *J. Micromech. Microeng.*, 2006, **16**, 341-348.

Lab on a Chip Accepted Manuscript